User's Manual for

Diffuser

v1.1

A program for diffusion modeling

Released March 30, 2022

Updated October, 28, 2025

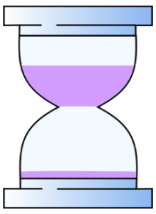

www.geoapp.cn

Li-Guang Wu, Yang Li, Michael C. Jollands, Pieter Vermeesch, Xian-Hua Li, 2022. Diffuser: a user-friendly program for diffusion chronometry with robust uncertainty estimation. Computers and Geosciences.
https://doi.org/10.1016/j.cageo.2022.105108

Contact: wlg@cugb.edu.cn (L.G. Wu) and geoliy@outlook.com (Y. Li)

Table of Contents

2022.9.19 update: add references of diffusivity used in Diffuser
2022.11.17 update: 1) add tips on the buttons and panels of the web app (move mouse towards the button to see). 2) add a template file for downloading.
2025.10.28 update: add a function to automatically calculate a specific cooling rate and its corresponding timescale at which diffusion just ceases at the measured profile.

Diffuser is a program written in MATLAB to model elemental diffusion in minerals. It is coded with robust uncertainty propagation of curve fitting, temperature, and experimentally determined diffusion coefficients. A web version is recommended for all users and available at http://www.geoapp.cn/. Diffuser can also be downloaded and installed from https://github.com/liguangwu/diffuser.git.

A user manual is given below.

1 Import data

1.1 Upload file

For running Diffuser directly in MATLAB, the user can run 'Diffuser.mlapp' or type 'Diffuser' in the MATLAB command window. After opening the graphical user interface (GUI) of Diffuser, the user can click the '**Select file**' button from the import data panel to import data (Figure 1).

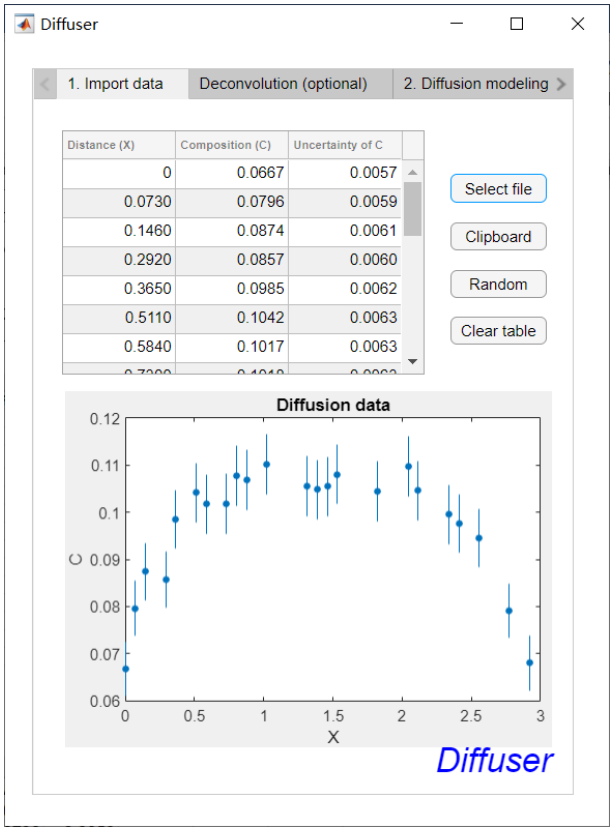

Figure 1. Import data panel of Diffuser

The measured diffusion profile can be fed into the software through a delimited text (e.g., txt or csv format), spreadsheet file (Microsoft® Excel), or clipboard (by the '**clipboard**' button; Figure 1). The distance and composition data should be in two columns (Figure 2). If composition uncertainties (σ) are assigned in another column (Figure 3), Diffuser will ask the user to input the column names of x, C, and σ (Figure 4). Otherwise, all composition data will be treated with equal weights. After data import, the data is directly visualized by means of a pre-formatted plot (Figure 1).

1.2 Other options

To play with Diffuser, the user can click the '**Random**' button (Figure 1) and Diffuser will generate a random diffusion profile. Then the user can deal with the example data in the same way. For clearing the table and plot of diffusion data, just click the '**Clear table**' button (Figure 1).

	A	B	C	D	E	F
1	Rubin et al., 2007	Fig. 1, Peak 2	put uncertainty in third column if you have			
2	X(m)	7Li ppb				
3	3.401E-05	0.000				
4	3.470E-05	1.187				
5	3.500E-05	0.591				
6	3.569E-05	1.778				
7	3.598E-05	0.000				
8	3.668E-05	1.179				
9	3.707E-05	3.534				
10	3.737E-05	6.524				
11	3.806E-05	6.553				
12	3.836E-05	16.015				
13	3.905E-05	25.248				
14	3.935E-05	48.689				
15	4.004E-05	75.149				

Figure 2. A diffusion profile containing two-column data.

	A	B	C	D	E	F
1	x (mm)	CaO (wt%)	1s			
2	0	0.0667	0.0057			
3	0.073	0.0796	0.0059			
4	0.146	0.0874	0.0061			
5	0.292	0.0857	0.006			
6	0.365	0.0985	0.0062			
7	0.511	0.1042	0.0063			
8	0.584	0.1017	0.0063			
9	0.73	0.1018	0.0063			
10	0.803	0.1077	0.0064			

Figure 3. A diffusion profile containing three-column data.

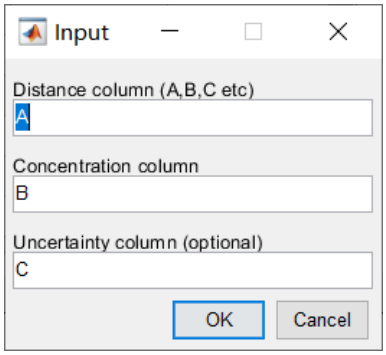

Figure 4. A pop-up window to input the column names of x, C, and σ.

2 Deconvolute the beam effect (optional)

Why and when the user needs deconvolution: All in-situ analytical techniques have a non-zero beam size, so the measured diffusion profiles will suffer from convolution to some degree, especially when the diffusion length approaches the resolution of the analytical technique. Jollands (2020) has developed a program for numerically deconvoluting diffusion profiles acquired using techniques with Gaussian, Lorentzian, (pseudo-)Voigt, circular/elliptical, or square/rectangular interaction volumes (PACE-the Program for Assessing Convolution Effects), which has been incorporated into Diffuser directly.

2.1 Choose deconvolution

The user can evaluate the convolution effect and determine whether deconvolution is necessary by ticking the box of '**Deconvolute analytical beam effects**' on the 'Deconvolution' panel (Figure 5).

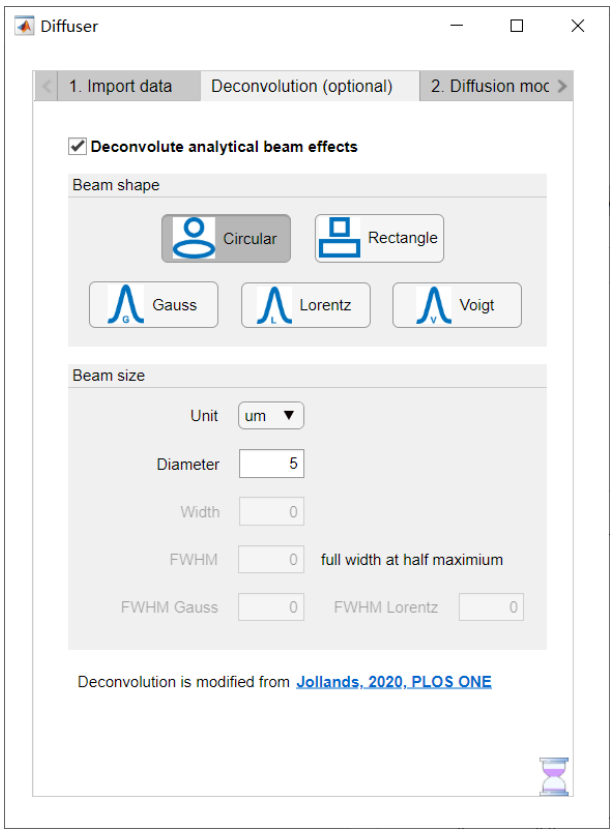

Figure 5. Deconvolution panel of Diffuser

2.2 Set the beam shape and size

If deconvolution is chosen, the beam shape and size and the **size unit** should be set (Figure 5). If a **circular/elliptical** beam shape is selected, the **diameter** of the beam is required. If a **square/rectangular** beam shape is selected, the **width** of the beam is required. If a **Gaussian or Lorentzian** beam shape is selected, the **full width of half maximum** (FWHM) of the beam is required. If a **pseudo-Voigt** beam shape is selected, the **FWHM of both the Gaussian and Lorentzian** components is needed. After the beam shape and size are set, Diffuser will deconvolute the diffusion profile to calculate the timescale.

3 Diffusion modeling

3.1 Set the unit of position *x*

After diffusion data import, the **unit of position *x*** should be set on the diffusion modeling panel (Figure 6), choosing from nm, μm, mm, and m. It should be emphasized that a wrong unit of *x* can lead to an unusual timescale which should be carefully checked.

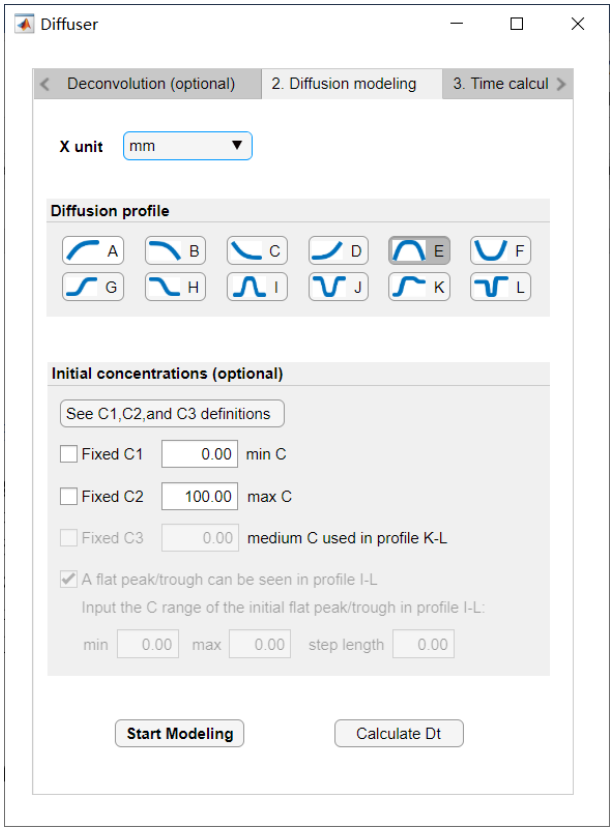

Figure 6. Diffusion modeling panel of Diffuser.

3.2 Choose the shape of the diffusion profile

The user can choose the relevant solution to Fick's second law graphically (i.e., determine which shape matches the input diffusion profile) by comparing the shape of the measured data profile with diffusion shapes in Figure 6.

3.3 Set the initial concentrations (optional)

The **initial compositions (C_1, C_2, and C_3)** can be fixed or determined automatically by curve fitting. Definitions of C_1, C_2, and C_3 (Figure 7) can be looked up through the '**See**

***C*$_1$, *C*$_2$, and *C*$_3$ definitions**' button.

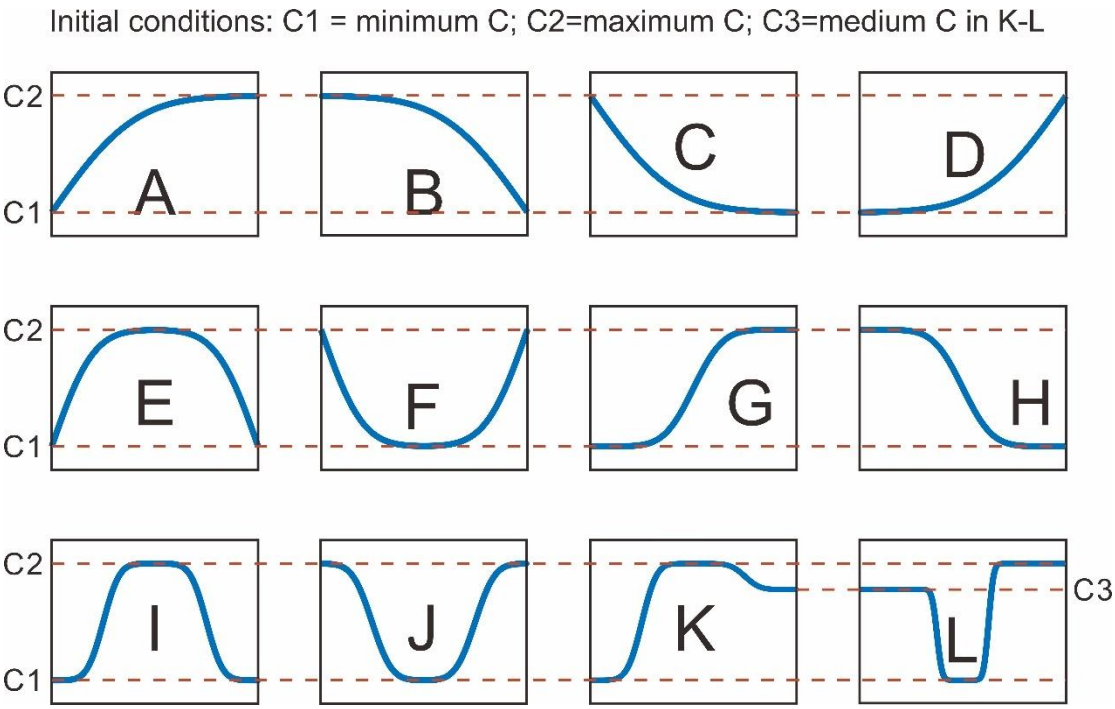

Figure 7. Definitions of initial compositions (C_1, C_2, and C_3) in Diffuser.

Specifically, if the user does not define an initial flat peak or trough for profiles I–L because it may be erased by diffusion (i.e., no tick in the box of '**a flat peak/trough can be seen in profile I-L**'), more parameters including **minimum and maximum values and a step length of the assumed flat peak or trough (*C*$_0$)** are required (Figure 8). In this case, Diffuser will plot the calculated *Dt* values vs. assumed initial flat compositions (Figure 9) after diffusion modeling (see section 3.4).

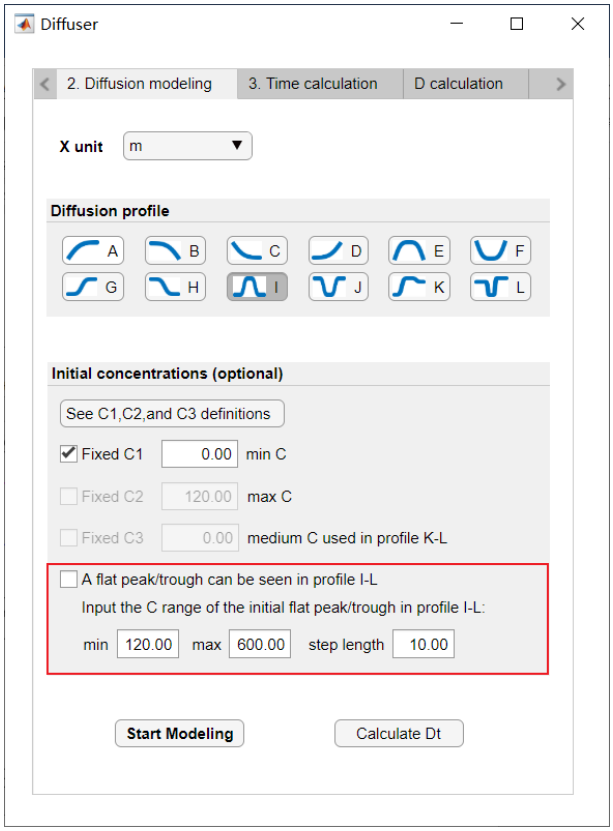

Figure 8. Minimum and maximum values and a step length of the assumed flat peak or trough for profiles I–L.

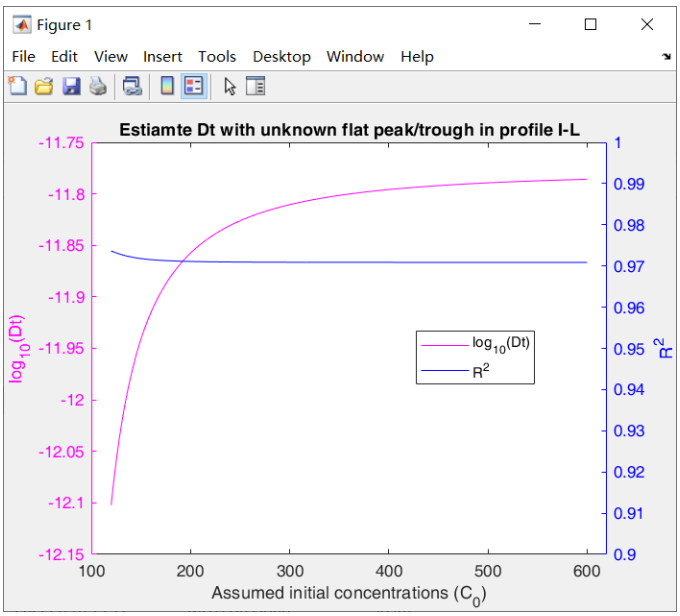

Figure 9. Estimate *Dt* with an assumed composition range of the initial flat peak/trough for profiles I–L.

3.4 Diffusion modeling results

The user can click the button '**Start modeling**' to make curve fitting and acquire a modeled *Dt* value (Figure 10). The curve fitting results can be saved in an independent file (Figure 11) through the button '**Calculate Dt**'. The user can evaluate the diffusion data quality through the goodness of fit (R^2). Usually, a low R^2 value (e.g., <0.8) indicates that the curve fitting of the diffusion profile will contribute to a large uncertainty of the timescale. Such a diffusion profile may not be good or valid to further calculate the timescale.

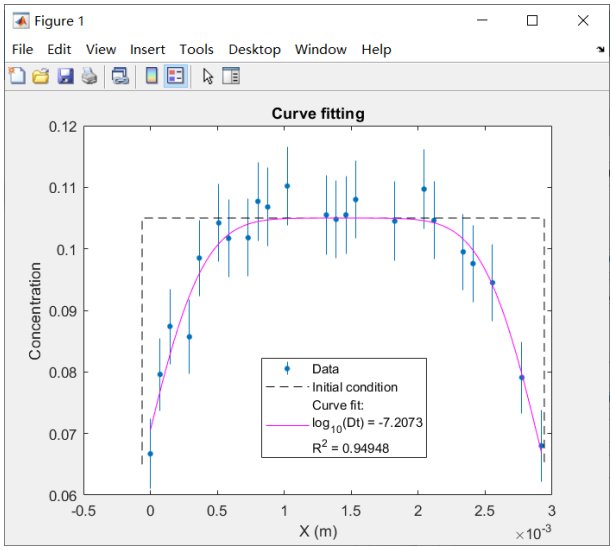

Figure 10. Curve fitting of the diffusion profile.

	A	B	C	D	E	F	G	H	I	J
1	Trials	R2	C1	C2	x0 (m)	rim-to-core length (m)	log10(Dt)	2s	Dt	2s
2	1	0.949479683	0.065	0.105	0.001439735	0.001501448	-7.207316696	0.169266205	6.20416E-08	2.41807E-08
3										

Figure 11. Curve fitting result of the diffusion profile.

4 Timescale or cooling rate calculation

4.1 Set the diffusion coefficient

To model timescales in natural samples, the diffusion coefficient should be set on the time calculation panel **using an Arrhenius equation for *D*** (Figure 12A) or **a constant *D*** (Figure 12B). If using an Arrhenius equation for *D*, the user can choose the targeted **mineral, element, and reference** (Figure 12A). Diffusion coefficient data collected from the literature are provided in a built-in excel file ('DiffusionCoefficient.xlsx', Figure 13). The program will read it automatically and users can access them via a drop-list on the diffusion coefficient panel (Figure 12A) once the program interface is opened.

Currently, Diffuser contains a library of diffusion coefficients for the following systems: olivine (Ca, Al, P, REE, Ti, H, Li, Be), garnet (Hf, REE, H), quartz (Ti, Al, H), zircon (REE, Ti, Al, Li), orthopyroxene (REE, Ti, Cr, H), clinopyroxene (Ti, REE, H), and feldspar (Sr, Ba, REE, H). These have been compiled in Diffuser by refitting original experimental data in previous studies. Thus, the algorithm of parameter uncertainties in Diffuser is internally consistent. Diffusion coefficients from other systems can be added into Diffuser by modifying the relevant template file. Requests to add other diffusion coefficients to future web versions of Diffuser can be sent to the first author (wlg@cugb.edu.cn).

If using an Arrhenius equation for D, the user also can choose uncertainty propagation of experimentally determined parameters D_0 and E_a (by ticking the box of '**Calculate with D_0 and E_a errors**') to see the contributions to the calculated timescale uncertainty compared with curve fitting and temperature uncertainties (see section 4.3).

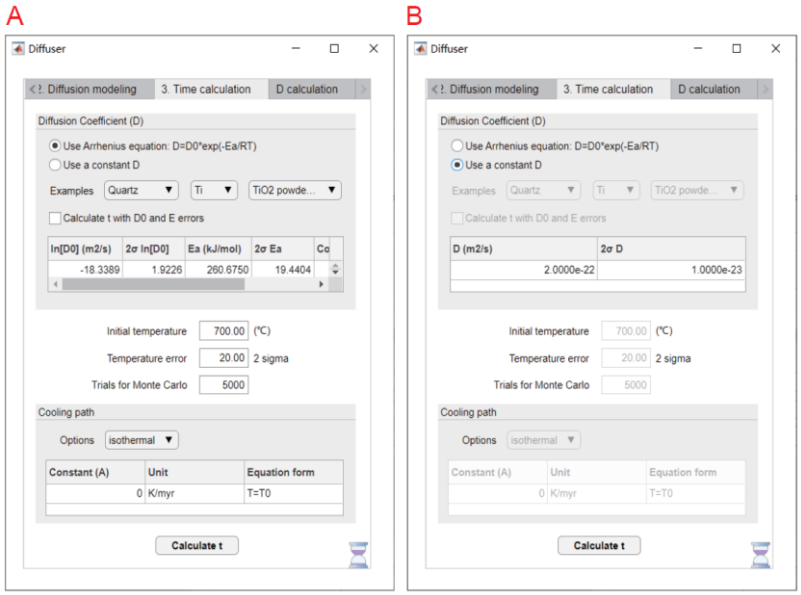

Figure 12. Time calculation panel of Diffuser.

	A	B	C	D	E	F	G	H
1	**Mineral**	**Element**	**Reference**	**ln(D0) (m^2/s)**	**2σ ln(D0)**	**E (kJ/mol)**	**2σ E (kJ/mol)**	**Covariance (ln(D0),E)**
2	Quartz	Ti	//[001], Cherniak et al. (2007), Chem. Geol.	-16.27	1.83	275.66	18.86	8.58
3	Quartz	Ti	//[001], Jollands et al. (2020), Geology	-19.21	2.74	310.61	34.48	23.42
4	Quartz	Al	Tailby et al. (2018), Am. Mineral.	-24.85	8.61	196.65	75.98	163.35
5	Zircon	Li	Trail et al. (2016) and Cherniak and Watson (2010), Contrib.	-13.85	2.08	278.27	19.93	10.34
6	Olivine	P	//[010], Watson et al. (2015), Am. Mineral.	-22.96	3.03	230.35	26.86	20.33
7	Olivine	Ca	//[100], Bloch et al. (2019), Geochim. Cosmochim. Acta	-19.34	1.38	250.05	13.87	4.75
8	Olivine	Ca	//[100], log[fO2]=-10 (bars), Coogan et al. (2005), Geochim. (	-20.19	3.19	233.64	40.25	31.99
9	Olivine	Ca	//[010], log[fO2]=-10 (bars), Coogan et al. (2005), Geochim. (	-23.59	2.54	189.64	32.02	20.25
10	Olivine	Ca	//[001], log[fO2]=-10 (bars), Coogan et al. (2005), Geochim. (	-23.20	3.54	188.40	44.84	39.55
11	Olivine	Al	//[100] (fo+en+crd), log[fO2]=-0.68, Zhukova et al. (2017), Cc	-2.86	12.50	367.63	164.74	514.36
12	Olivine	REE	Cherniak (2010), Am. Mineral.	-21.81	3.26	276.93	35.38	28.79
13	Olivine	REE	assumed a sensible E of 225±25 kJ/mol; Spandler and O'Ne	-17.88	3.84	225.00	25.00	23.77
14	Olivine	Ti	forsterite, Cherniak and Liang (2014), Geochim. Cosmochim.	-29.56	2.84	212.77	33.63	23.82
15	Olivine	Ti	San Carlos olivine, Cherniak and Liang (2014), Geochim. Cc	-31.36	2.67	196.81	31.72	21.12
16	Olivine	H	//[100], Jollands et al. (2016), Am. Mineral.	-6.28	3.52	229.92	32.80	28.84
17	Olivine	H	//[100], Demouchy and Mackwell (2003), Phys Chem Mineral	-9.90	3.68	225.00	40.00	36.47
18	Olivine	H	//[100], Kohlstedt and Mackwell (1998), Zeitschrift für Physik	-8.88	5.26	144.81	50.87	66.71
19	Olivine	H	//[010], Demouchy and Mackwell (2003), Phys Chem Mineral	-10.59	2.76	205.00	31.00	21.20
20	Olivine	H	//[010], Kohlstedt and Mackwell (1998), Zeitschrift für Physik	-8.23	10.44	185.87	103.02	268.46
21	Olivine	H	//[001], Jollands et al. (2016), Am. Mineral.	-5.29	1.95	220.69	17.54	8.50
22	Olivine	H	//[001], Demouchy and Mackwell (2003), Phys Chem Mineral	-8.75	2.99	210.00	33.00	24.45
23	Olivine	H	//[001], Kohlstedt and Mackwell (1998), Zeitschrift für Physik	-16.40	9.92	103.69	97.83	242.20
24	Olivine	Li	//[001], interstitial site, Dohmen et al. (2010), Geochim. Cosm	-5.34	1.23	214.24	12.50	3.82
25	Olivine	Li	//[001], octahedral site, Dohmen et al. (2010), Geochim. Cosi	-15.38	5.53	188.04	56.10	76.91
26	Olivine	Be	//[001], Jollands et al. (2016), Earth Planet. Sci. Lett.	-13.06	0.71	231.96	8.55	1.52

Figure 13. Library of diffusion coefficients in Diffuser.

4.2 Set the temperature condition

The **initial temperature with its uncertainty** when diffusion starts**, trials for the Monte Carlo calculation, and cooling path (isothermal, linear, exponential, or parabolic)** should be set on the time calculation panel.
If the user selects an isothermal diffusion history for the 'cooling path', the program will calculate a constant D using the input initial temperature. If selecting a linear, exponential, or parabolic cooling path with **a known cooling rate**, the user should input the constant coefficient (A) in the form of:

$T=T_0$-At for linear cooling
$T=T_0e^{-At}$ for exponential cooling
$T=T_0$-At^2 for parabolic cooling

If a non-isothermal condition is set and **the cooling rate is unknown** (on the Time calculation panel), Diffuser will automatically determine the cooling rate and calculate the corresponding shortest timescale at which diffusion ceases at the measured profile.

4.3 Timescale results

After parameters are set, the user can start calculating the timescale through the button '**Calculate t**'. If the temperature is assigned a non-zero error, a marginal plot will show distributions of the temperature and diffusion timescale and the trade-off between these two parameters (Figure 14). Otherwise, only a histogram will show the distributions of the timescale (Figure 15). A histogram will also show the uncertainty budget of the modeled timescale (Figure 16). so that the user can evaluate the main contributions of the timescale uncertainty. This helps users find more ways for better timescale constraints, e.g., a diffusion profile with a better R^2 value of curve fitting, a more precious method of temperature estimation, or a diffusive element with a more precious diffusion coefficient.

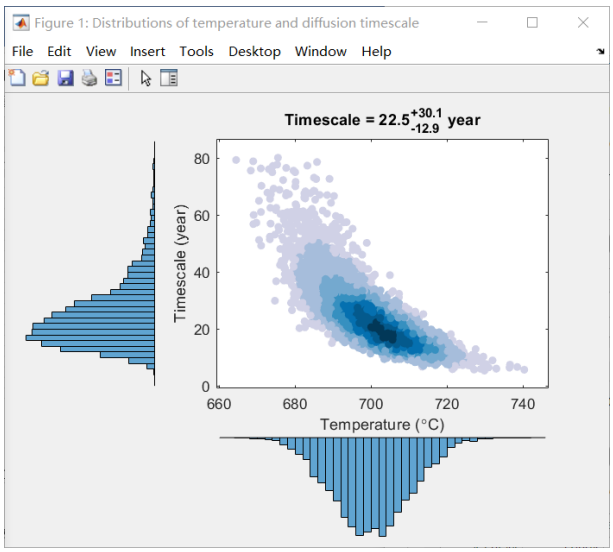

Figure 14. Marginal plot showing distributions of the temperature and diffusion timescale when the temperature is assigned a non-zero error.

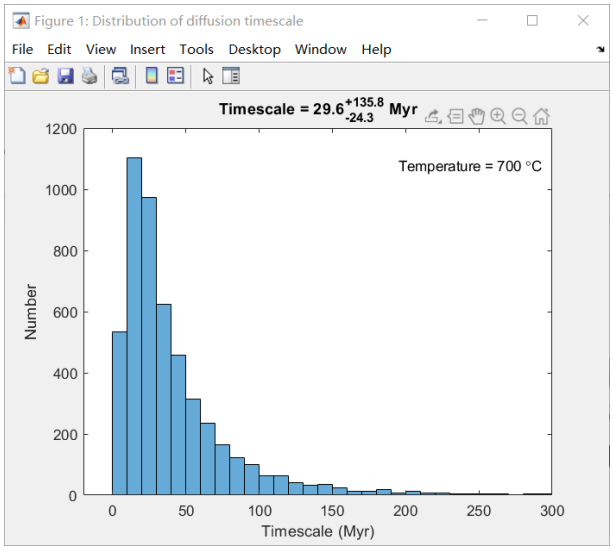

Figure 15. Histogram showing the distribution of the modeled timescale when the temperature is assigned an error of zero.

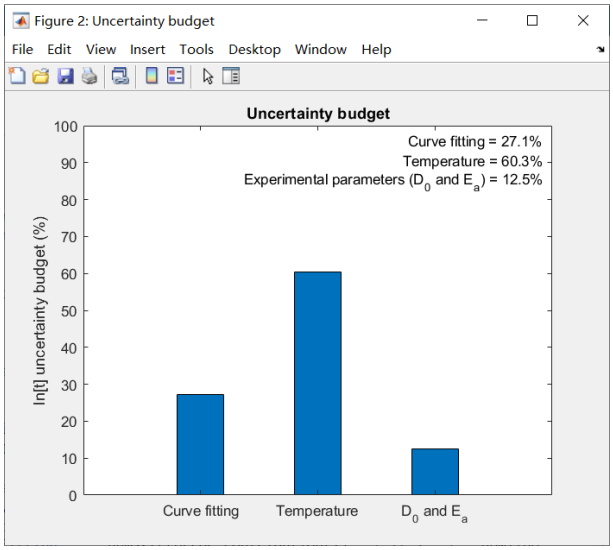

Figure 16. Histogram showing the uncertainty budget of the modeled timescale.

If the temperature decreases with time (non-isothermal systems), Monte Carlo results of timescales are displayed on histograms to show whether they are log-normally distributed based on the Lilliefors test (Figure 17). If not, the user should consider using a larger number of trials for Monte Carlo modeling. A dialog will appear saying that 'Trials are not enough to estimate ln[t] uncertainty budget' (Figure 18) when the calculated uncertainty of the timescale using propagation of three error sources (curve fitting, temperature, and D_0 and E_a) is even smaller than that using propagation of two error sources (or two sources<one source). In this case, the user also should consider

using a larger number of trials for Monte Carlo modeling.

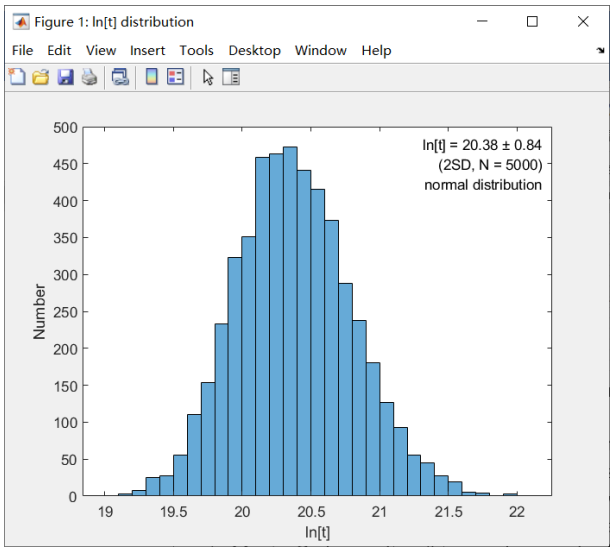

Figure 17. Histogram showing whether ln[t] are log-normally distributed for non-isothermal diffusion modeling.

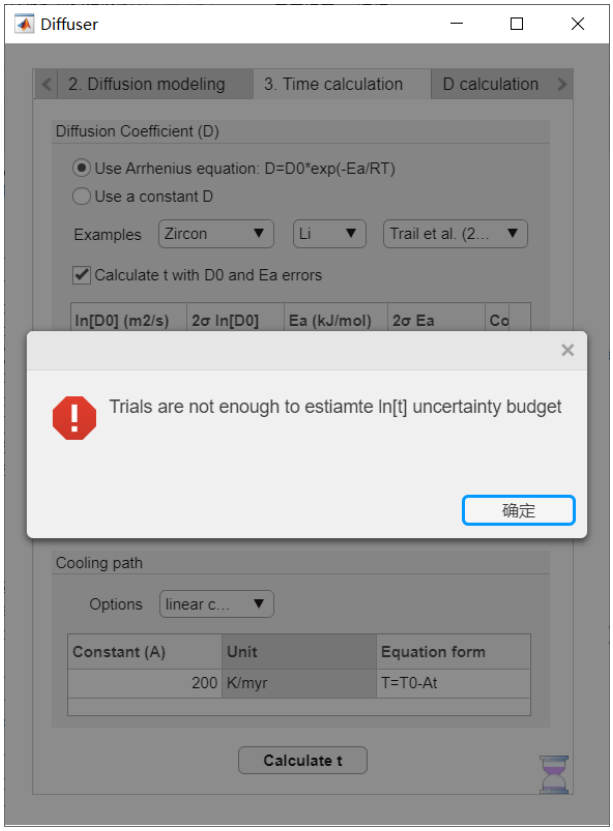

Figure 18. A dialog showing that trials of Monte Carlo are not enough for estimating the uncertainty budget.

Finally, the modeled timescale and Monte Carlo results can be saved in individual files (Figures 19 and 20) after clicking the button '**Calculate t**'. Specifically, if the user does

not define an initial flat peak or trough for profiles I–L, Diffuser will plot the modeled timescales vs. assumed initial flat compositions (Figure 21).

	A	B	C	D	E	F	G	H	I	J	K
1	Trials	R2	C1	C2	x0 (m)	half band width (m)	log10(Dt)	2s	Timescale (year)	-2s	+2s
2	1	0.973650013	0	120	4.17501E-05	2.07095E-06	-12.10230331	0.100196679	22.45246895	-12.85626035	30.08008665

Figure 19. Timescale results in Diffuser.

	A	B	C	D	E	F
1	Temperature (Celciu	log10(Dt)=-12.1023				
2		t(s), normal distribution				
3	710.7161606	622360713.6				
4	697.5291488	931498663.9				
5	682.472005	1340934549				
6	711.1874759	433521960.5				
7	701.281457	401655661.9				
8	715.9695517	364050624.4				
9	710.0678741	419741180.7				
10	708.4771519	516501900.9				
11	696.5475219	837155248.1				
12	708.7940009	492472844.6				
13	696.0567776	1002808464				
14	702.7083621	841303567.1				
15	699.355481	910018888.6				

Figure 20. Monte Carlo results in Diffuser.

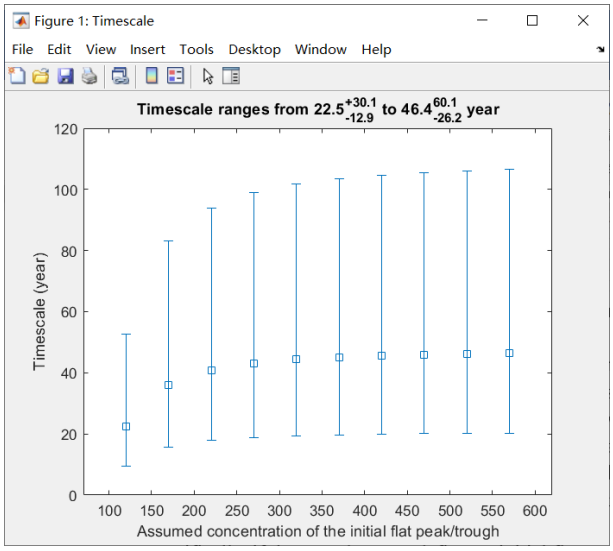

Figure 21. Timescales calculated for an assumed composition range of the flat peak/trough in profiles I–L.

4.4 Cooling rate results

If the cooling rate is not provided for non-isothermal conditions ('Cooling rate in known' checkbox is not ticked; Figure 22), Diffuser will automatically determine it and calculate the corresponding shortest timescale at which diffusion ceases at the measured profile.

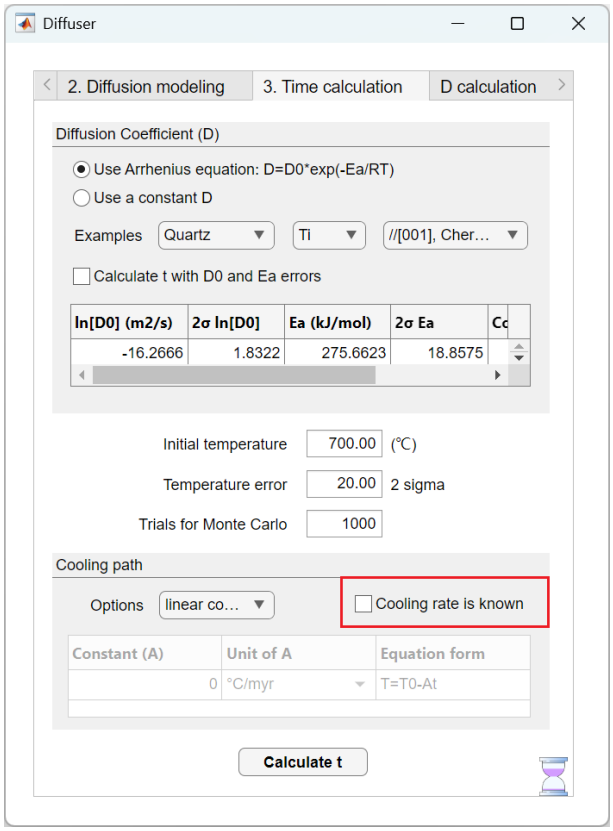

Figure 22. Cooling rate is unknown for non-isothermal conditions.

The Monte Carlo results of the cooling rate and its corresponding timescale will be shown in a figure (Figure 23) and saved in a file. An example of Ti diffusion in quartz in Watson and Cherniak (2015) is recalculated by Diffuser, which yields a cooling rate of ~63°C/kyr and a timescale of ~9 kyr after uncertainty propagation of curve fitting, temperature, and diffusivity. The former is consistent with an independent method of Watson and Cherniak (2015) (~74°C/kyr).

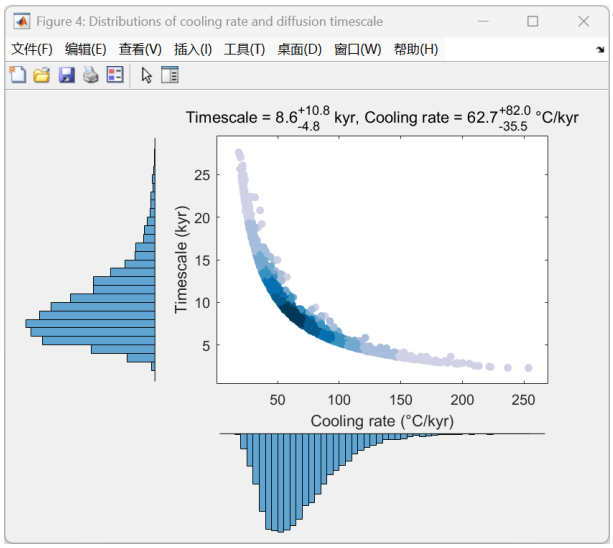

Figure 23. Monte Carlo results of the cooling rate and its corresponding timescale.

5 Diffusivity calculation (for experimental studies)

5.1 Calculate *D* for a specific temperature in a single experimental run

To calculate a diffusion coefficient in an isothermal experimental study, the user can input the **experimental duration** on the diffusivity calculation panel (Figure 24) and get an estimated *D* with its uncertainty (Figure 25) through the button '**Calculate D**'.

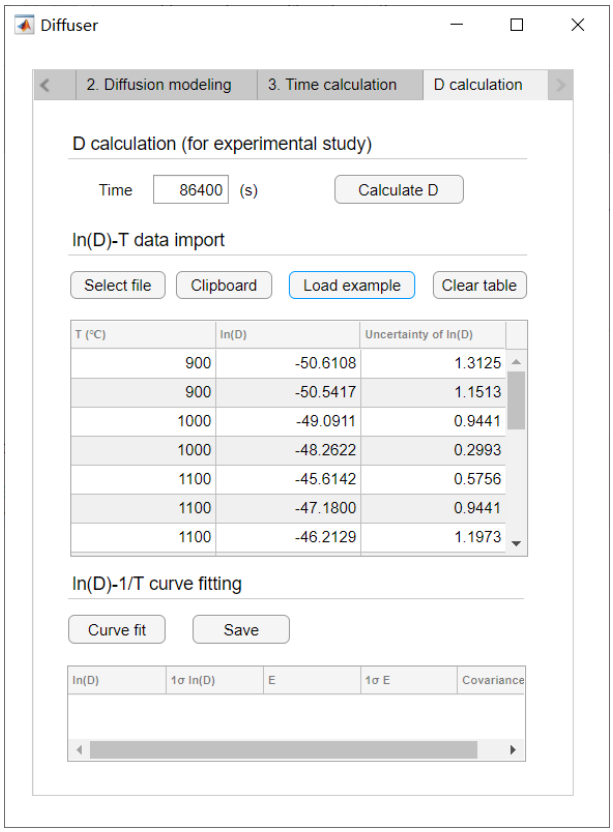

Figure 24. Diffusivity calculation panel of Diffuser

	A	B	C	D	E	F	G	H	I	J	K	L	M	N
1	Trials	R2	C1	C2	x0 (m)	half band width (m)	log10[Dt]	2s	log10[D]	2s	ln[D]	2s	D	2s
2	1	0.973650013	0	120	4.17501E-05	2.07095E-06	-12.10230331	0.10019668	-20.90213991	0.10019668	-48.12895576	0.230711379	1.25274E-21	2.89021E-22
3														

Figure 25. *D* calculation results in Diffuser.

5.2 Calculate D_0 and E_a for a whole experiment

The user can import all experimental data by the '**Select file**' button (ln[*D*] at different temperatures; Figure 24), through a delimited text (e.g., txt or csv format), spreadsheet file (Microsoft® Excel), or clipboard (by the 'clipboard' button). The temperature and ln[*D*] data should be in two columns. If ln[*D*] uncertainties are assigned in another column, Diffuser will ask the user to input the column names of temperature, ln[*D*], and uncertainties. Otherwise, all ln[*D*] data will be treated with equal weights.

After data import, the user can calculate the parameters of ln[D_0] and E_a in the diffusion coefficient and their covariance by ordinary linear least-squares regression (Figure 26) through the button '**Curve fit**'. The curve fitting result also can be saved in an independent file (Figure 27) through the button '**Save**'.

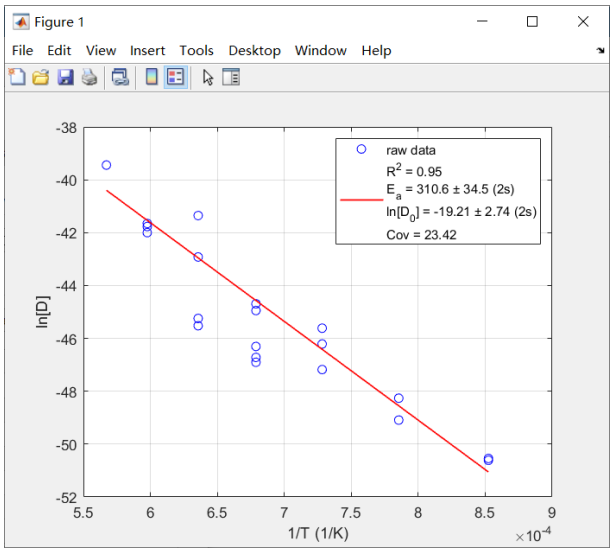

Figure 26. Curve fitting of ln[D] and 1/T.

	A	B	C	D	E
1	ln[D0] (m2/s)	2s ln[D0]	Ea (kJ/mol)	2s Ea	Covariance (ln[D0],Ea)
2	-19.2071108	2.74027404	310.6069714	34.48358696	23.42240413
3					

Figure 27. Curve fitting result of ln[D] and 1/T.

5.3 Other options

To play with Diffuser, the user can click the '**Load example**' button (Figure 24) and Diffuser will generate an example data of ln[D] at different temperatures. Then the user can deal with the example data in the same way. For clearing the table and plot, just click the '**Clear table**' button (Figure 24).

6 Web version

A web version of Diffuser is available at http://www.geoapp.cn/. It has nearly the same functions as the offline version. However, it cannot import data from the clipboard (thus the clipboard button is removed; Figure 28). It also cannot show pop-up windows, so instead of reminding the user to select the sheet and input column names of x, C, and σ (Figure 4), it imports data directly by reading the first sheet and its first two or three columns (Figure 2 and 3).

All the figures of the web version can be downloaded as portable document formats (‘**Save figures**’ button) so that the user can modify it easily offline.

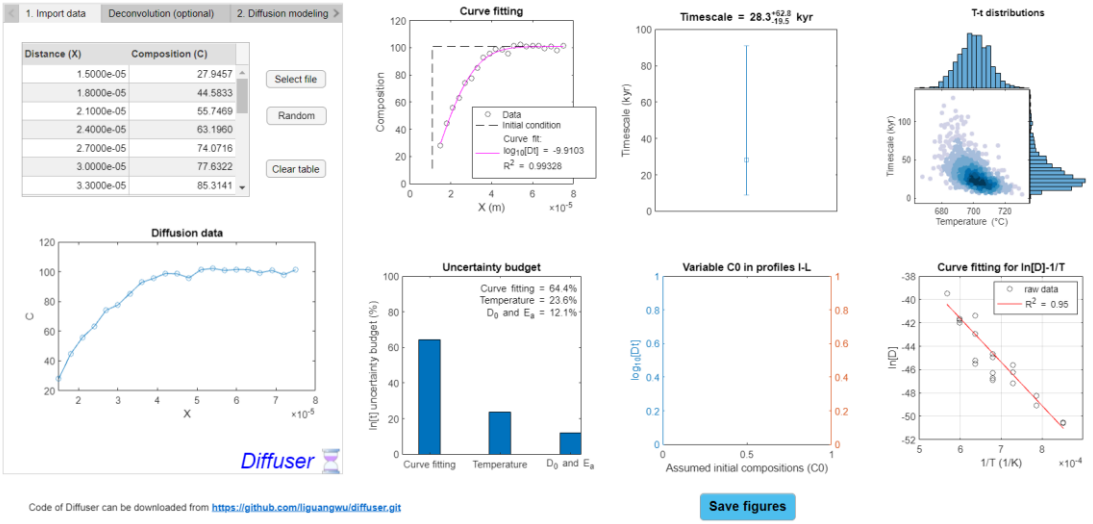

Figure 28. The web version of Diffuser.

7 References of diffusivity

Clinopyroxene

Cherniak, D.J., Liang, Y., 2012. Ti diffusion in natural pyroxene. Geochimica Et Cosmochimica Acta 98, 31–47. https://doi.org/10.1016/j.gca.2012.09.021

Ingrin, J., Hercule, S., Charton, T., 1995. Diffusion of hydrogen in diopside: Results of dehydration experiments. Journal of Geophysical Research: Solid Earth 100, 15489–15499. https://doi.org/10.1029/95JB00754

Müller, T., Dohmen, R., Becker, H.W., ter Heege, J.H., Chakraborty, S., 2013. Fe–Mg interdiffusion rates in clinopyroxene: experimental data and implications for Fe–Mg exchange geothermometers. Contributions to Mineralogy and Petrology 166, 1563–1576. https://doi.org/10.1007/s00410-013-0941-y

Sundvall, R., Skogby, H., Stalder, R., 2009. Hydrogen diffusion in synthetic Fe-free diopside. European Journal of Mineralogy 21, 963–970. https://doi.org/10.1127/0935-1221/2009/0021-1971

Van Orman, J.A., Grove, T.L., Shimizu, N., 2001. Rare earth element diffusion in diopside: influence of temperature, pressure, and ionic radius, and an elastic model for diffusion in silicates. Contributions to Mineralogy and Petrology 141, 687–703. https://doi.org/10.1007/s004100100269

Feldspar

Behrens, H., Johannes, W., Schmalzried, H., 1990. On the mechanisms of cation diffusion processes in ternary feldspars. Physics and Chemistry of Minerals 17, 62–78. https://doi.org/10.1007/BF00209227

Cherniak, D.J., 1996. Strontium diffusion in sanidine and albite, and general comments on strontium diffusion in alkali feldspars. Geochimica Et Cosmochimica Acta 60, 5037–5043. https://doi.org/10.1016/S0016-7037(96)00293-1

Cherniak, D.J., 2002. Ba diffusion in feldspar. Geochimica Et Cosmochimica Acta 66, 1641–1650. https://doi.org/10.1016/S0016-7037(01)00866-3

Cherniak, D.J., 2003. REE diffusion in feldspar. Chemical Geology 193, 25–41. https://doi.org/10.1016/S0009-2541(02)00246-2

Cherniak, D.J., Watson, E.B., 2020. Ti diffusion in feldspar. American Mineralogist 105, 1040-1051. https://doi.org/10.2138/am-2020-7272

Giletti, B.J., Shanahan, T.M., 1997. Alkali diffusion in plagioclase feldspar. Chemical Geology 139, 3–20. https://doi.org/10.1016/S0009-2541(97)00026-0

Johnson, E.A., Rossman, G.R., 2013. The diffusion behavior of hydrogen in plagioclase feldspar at 800–1000 °C: Implications for re-equilibration of hydroxyl in volcanic phenocrysts. American Mineralogist 98, 1779–1787. https://doi.org/10.2138/am.2013.4521

Pohl, F., Behrens, H., Oeser, M., Marxer, F., Dohmen, R., 2024. Li diffusion in plagioclase crystals and glasses – implications for timescales of geological processes. European Journal of Mineralogy 36, 985–1003. https://doi.org/10.5194/ejm-36-985-2024

Pohl, F., 2025. Diffusion of major and trace elements in plagioclase, Naturwissenschaftlichen Fakultät. Leibniz University Hannover, Hannover, Germany, p. 176.

Garnet

Bloch, E., Ganguly, J., Hervig, R., Cheng, W., 2015. ^{176}Lu–^{176}Hf geochronology of garnet I: experimental determination of the diffusion kinetics of Lu^{3+} and Hf^{4+} in garnet, closure temperatures and geochronological implications. Contributions to Mineralogy and Petrology 169, 12. https://doi.org/10.1007/s00410-015-1109-8

Bloch, E.M., Jollands, M.C., Devoir, A., Bouvier, A.-S., Ibañez-Mejia, M., Baumgartner, L.P., 2020. Multispecies Diffusion of Yttrium, Rare Earth Elements and Hafnium in Garnet. Journal of Petrology 61, egaa055. https://doi.org/10.1093/petrology/egaa055

Carlson, W.D., 2012. Rates and mechanism of Y, REE, and Cr diffusion in garnet. American Mineralogist 97, 1598–1618. https://doi.org/10.2138/am.2012.4108

Cherniak, D., 2005. Yb and Y diffusion in grossular garnet. Goldschmidt Conference Abstract, A405.

Tirone, M., Ganguly, J., Dohmen, R., Langenhorst, F., Hervig, R., Becker, H.-W., 2005. Rare earth diffusion kinetics in garnet: Experimental studies and applications. Geochimica Et Cosmochimica Acta 69, 2385–2398. https://doi.org/10.1016/j.gca.2004.09.025

Van Orman, J.A., Grove, T.L., Shimizu, N., Layne, G.D., 2002. Rare earth element diffusion in a natural pyrope single crystal at 2.8 GPa. Contributions to Mineralogy and Petrology 142, 416–424. https://doi.org/10.1007/s004100100304

Scicchitano, M.R., Jollands, M.C., Williams, I.S., Hermann, J., Rubatto, D., Kita, N.T., Nachlas, W.O., Valley, J.W., Escrig, S., Meibom, A., 2022. Oxygen diffusion in garnet: Experimental calibration and implications for timescales of metamorphic processes and retention of primary O isotopic signatures. American Mineralogist 107, 1425–1441. https://doi.org/10.2138/am-2022-7970

Olivine

Bloch, E.M., Jollands, M.C., Gerstl, S.S.A., Bouvier, A.S., Plane, F., Baumgartner, L.P., 2019. Diffusion of calcium in forsterite and ultra-high resolution of experimental diffusion profiles in minerals using local electrode atom probe tomography. Geochimica Et Cosmochimica Acta 265, 85–95. https://doi.org/10.1016/j.gca.2019.09.003

Cherniak, D.J., 2010. REE diffusion in olivine. American Mineralogist 95, 362–368. https://doi.org/10.2138/am.2010.3345

Cherniak, D.J., Liang, Y., 2014. Titanium diffusion in olivine. Geochimica Et Cosmochimica Acta 147, 43–57. https://doi.org/10.1016/j.gca.2014.10.016

Coogan, L.A., Hain, A., Stahl, S., Chakraborty, S., 2005. Experimental determination of the diffusion coefficient for calcium in olivine between 900°C and 1500°C. Geochimica Et Cosmochimica Acta 69, 3683–3694. https://doi.org/10.1016/j.gca.2005.03.002

Demouchy, S., Mackwell, S., 2003. Water diffusion in synthetic iron-free forsterite. Physics and Chemistry of Minerals 30, 486–494. https://doi.org/10.1007/s00269-003-0342-2

Dohmen, R., Kasemann, S.A., Coogan, L., Chakraborty, S., 2010. Diffusion of Li in olivine. Part I: Experimental observations and a multi species diffusion model. Geochimica Et Cosmochimica Acta 74, 274–292. https://doi.org/10.1016/j.gca.2009.10.016

Jollands, M.C., Burnham, A.D., O'Neill, H.S.C., Hermann, J., Qian, Q., 2016. Beryllium diffusion in olivine: A new tool to investigate timescales of magmatic processes. Earth and Planetary Science Letters 450, 71–82. https://doi.org/10.1016/j.epsl.2016.06.028

Jollands, M.C., Padrón-Navarta, J.A., Hermann, J., O'Neill, H.S.C., 2016. Hydrogen diffusion in Ti-doped forsterite and the preservation of metastable point defects. American Mineralogist 101, 1571–1583. https://doi.org/10.2138/am-2016-55681571

Kohlstedt, D.L., Mackwell, S.J., 1998. Diffusion of hydrogen and intrinsic point defects in olivine. Zeitschrift für physikalische Chemie 207, 147–162. https://doi.org/10.1524/zpch.1998.207.Part_1_2.147

Spandler, C., O'Neill, H.S.C., 2010. Diffusion and partition coefficients of minor and trace elements in San Carlos olivine at 1,300°C with some geochemical implications. Contributions to Mineralogy and Petrology 159, 791–818. https://doi.org/10.1007/s00410-009-0456-8

Watson, E.B., Cherniak, D.J., Holycross, M.E., 2015. Diffusion of phosphorus in olivine and molten basalt†. American Mineralogist 100, 2053–2065. https://doi.org/10.2138/am-2015-5416

Zhukova, I., O'Neill, H., Campbell, I.H., 2017. A subsidiary fast-diffusing substitution mechanism of Al in forsterite investigated using diffusion experiments under controlled thermodynamic conditions. Contributions to Mineralogy and Petrology 172, 53. https://doi.org/10.1007/s00410-017-1365-x

Orthopyroxene

Cherniak, D.J., Liang, Y., 2007. Rare earth element diffusion in natural enstatite. Geochimica Et Cosmochimica Acta 71, 1324–1340. https://doi.org/10.1016/j.gca.2006.12.001

Cherniak, D.J., Liang, Y., 2012. Ti diffusion in natural pyroxene. Geochimica Et Cosmochimica Acta 98, 31–47. https://doi.org/10.1016/j.gca.2012.09.021

Demers-Roberge, A., Jollands, M.C., Tollan, P., Müntener, O., 2021. H diffusion in orthopyroxene and the retention of mantle water signatures. Geochimica Et Cosmochimica Acta 305, 263–281. https://doi.org/10.1016/j.gca.2021.04.005

Ganguly, J., Ito, M., Zhang, X., 2007. Cr diffusion in orthopyroxene: Experimental determination, 53Mn–53Cr thermochronology, and planetary applications. Geochimica Et Cosmochimica Acta 71, 3915–3925. https://doi.org/10.1016/j.gca.2007.05.023

Sano, J., Ganguly, J., Hervig, R., Dohmen, R., Zhang, X., 2011. Neodymium diffusion in orthopyroxene: Experimental studies and applications to geological and planetary problems. Geochimica Et Cosmochimica Acta 75, 4684–4698. https://doi.org/10.1016/j.gca.2011.05.040

Stalder, R., Behrens, H., 2006. D/H exchange in pure and Cr-doped enstatite: implications for hydrogen diffusivity. Physics and Chemistry of Minerals 33, 601–611. https://doi.org/10.1007/s00269-006-0112-z

Quartz

Audétat, A., Miyajima, N., Wiesner, D., Audinot, J.-N., 2021. Confirmation of slow Ti diffusion in quartz by diffusion couple experiments and evidence from natural samples. Geology 49, 963–967. https://doi.org/10.1130/G48785.1

Audétat, A., Schmitt, A.K., Njul, R., Saalfeld, M., Borisova, A., Lu, Y., 2023. New constraints on Ti diffusion in quartz and the priming of silicic volcanic eruptions. Nature Communications 14, 4277. https://doi.org/10.1038/s41467-023-39912-5

Cherniak, D.J., Watson, E.B., Wark, D.A., 2007. Ti diffusion in quartz. Chemical Geology 236, 65–74. https://doi.org/10.1016/j.chemgeo.2006.09.001

Jollands, M.C., Bloch, E., Müntener, O., 2020. New Ti-in-quartz diffusivities reconcile natural Ti zoning with time scales and temperatures of upper crustal magma reservoirs. Geology 48, 654–657. https://doi.org/10.1130/G47238.1

Jollands, M.C., Ellis, B., Tollan, P.M.E., Müntener, O., 2020. An eruption chronometer based on experimentally determined H-Li and H-Na diffusion in quartz applied to the Bishop Tuff. Earth and Planetary Science Letters 551, 116560. https://doi.org/10.1016/j.epsl.2020.116560

Kronenberg, A.K., Kirby, S.H., Aines, R.D., Rossman, G.R., 1986. Solubility and diffusional uptake of hydrogen in quartz at high water pressures: Implications for hydrolytic weakening. Journal of Geophysical Research: Solid Earth 91, 12723–12741. https://doi.org/10.1029/JB091iB12p12723

Tailby, N.D., Cherniak, D.J., Watson, E.B., 2018. Al diffusion in quartz. American Mineralogist 103, 839–847. https://doi.org/10.2138/am-2018-5613

Zircon

Bloch, E.M., Jollands, M.C., Tollan, P., Plane, F., Bouvier, A.S., Hervig, R., Berry, A.J., Zaubitzer, C., Escrig, S., Müntener, O., Ibañez-Mejia, M., Alleon, J., Meibom, A., Baumgartner, L.P., Marin-Carbonne, J., Newville, M., 2022. Diffusion anisotropy of Ti in zircon and implications for Ti-in-zircon thermometry. Earth and Planetary Science Letters 578, 117317. https://doi.org/10.1016/j.epsl.2021.117317

Cherniak, D.J., Hanchar, J.M., Watson, E.B., 1997. Rare-earth diffusion in zircon. Chemical Geology 134, 289–301. https://doi.org/10.1016/S0009-2541(96)00098-8

Cherniak, D.J., Watson, E.B., 2007. Ti diffusion in zircon. Chemical Geology 242, 470–483. https://doi.org/10.1016/j.chemgeo.2007.05.005

Cherniak, D.J., Watson, E.B., 2010. Li diffusion in zircon. Contributions to Mineralogy and Petrology 160, 383–390. https://doi.org/10.1007/s00410-009-0483-5

Cherniak, D.J., 2021. Aluminum diffusion in zircon. Chemical Geology 584, 120510. https://doi.org/10.1016/j.chemgeo.2021.120510

Trail, D., Cherniak, D.J., Watson, E.B., Harrison, T.M., Weiss, B.P., Szumila, I., 2016. Li zoning in zircon as a potential geospeedometer and peak temperature indicator. Contributions to Mineralogy and Petrology 171, 25. https://doi.org/10.1007/s00410-016-1238-8

Titanite

Cherniak, D.J., 2006. Zr diffusion in titanite. Contributions to Mineralogy and Petrology 152, 639–647. https://doi.org/10.1007/s00410-006-0133-0

Cherniak, D.J., 2015. Nb and Ta diffusion in titanite. Chemical Geology 413, 44–50. https://doi.org/10.1016/j.chemgeo.2015.08.010